Cell Communication and Signaling

RESEARCH

Open Access

Identification of genetically engineered strategies to manipulate nano-platforms presenting immunotherapeutic ligands for alleviating primary ovarian insufficiency progression

Guannan Zhou[1,2*†], Yuanyuan Gu[1,2†], Menglei Zhang[1†], Jingxin Ding[1†], Guanming Lu[3,4†], Keqin Hua[1†] and Fang Shen[1†]

Abstract

Primary ovarian insufficiency (POI) is a pathological condition characterized by the early loss of functional ovarian follicles, leading to infertility and systemic consequences affecting reproductive, skeletal, cardiovascular, and neurocognitive helath. Aberrant immune activation, particularly an augmented T cell response in the ovary, plays a critical role in POI pathogenesis. In this context, therapeutic modulation of immune responses through immune checkpoint ligands has garnered interest. In the present study, we identified Lamp2b as an optimal scaffold for engineering extracellular vesicles (EVs). By genetically modifying HEK-293 T-derived EVs to present PD-L1 and Gal-9, enabling them to suppress ovarian autoreactive T lymphocytes and protect ovarian cells from immune-mediated destruction. Functionally, the bioengineered nanoplatform demonstrated potent immunosuppressive effects by promoting apoptosis of effector T cells, reducing intraovarian $CD8^+$ T cell infiltration and reinstating serum anti-Müllerian hormone (AMH) levels in POI models. These combined actions effectively halted disease progression, ultimately preventing POI progression and preserving ovarian function.

†Guannan Zhou, Yuanyuan Gu and Menglei Zhang contributed equally to this work.

†Guannan Zhou, Jingxin Ding, Guanming Lu, Keqin Hua and Fang Shen contributed equally to this work, as co-corresponding authors.

*Correspondence:
Guannan Zhou
zgnsmmu@163.com
Full list of author information is available at the end of the article

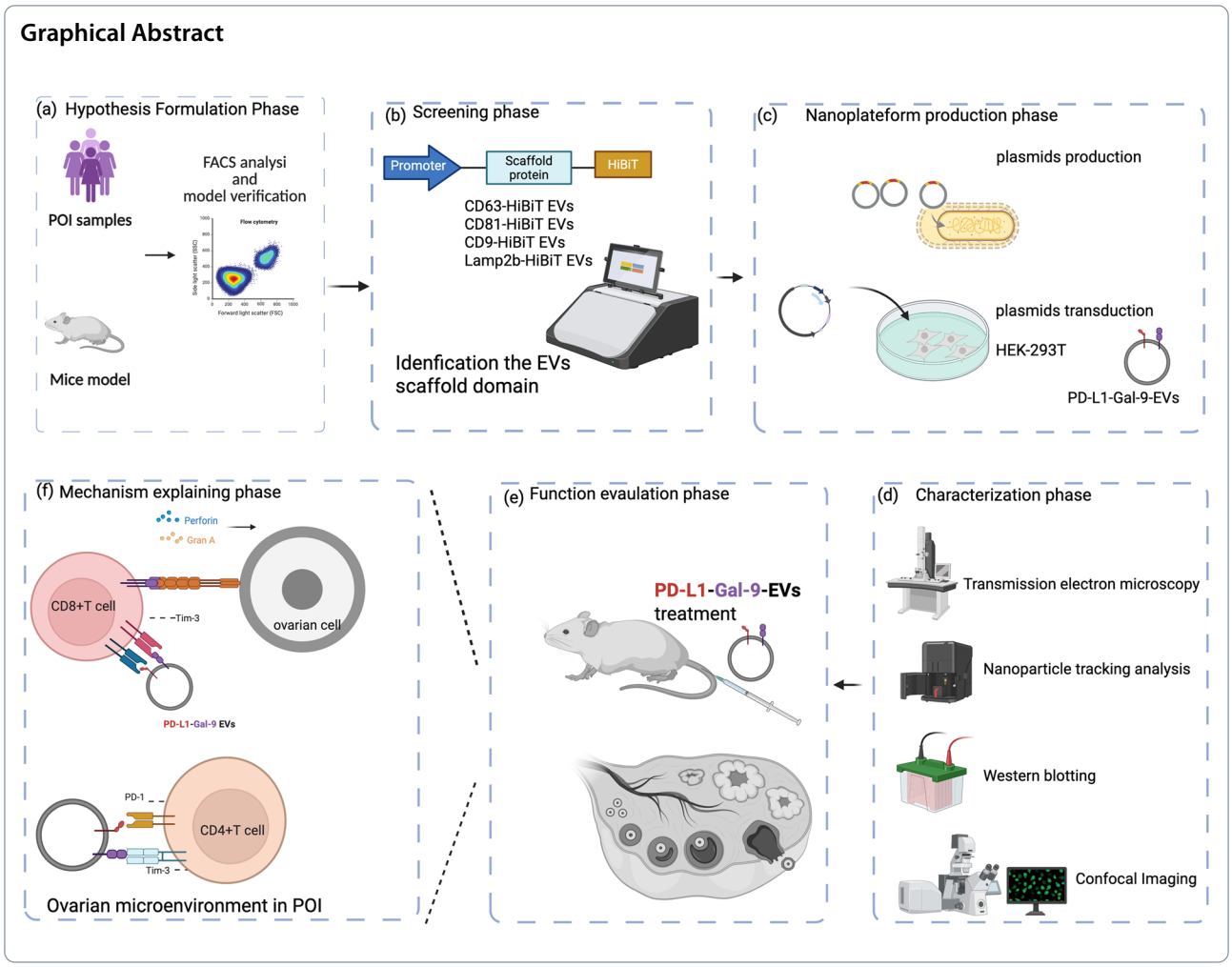

Background

Primary Ovarian Insufficiency (POI), also known as premature ovarian failure (POF), is a condition where ovarian function declines before the age of 40, leading to reduced estrogen production, menstrual irregularities, and infertility [1, 2]. Clinically, POI manifests with menstrual irregularities, infertility, depression [3] and symptoms of estrogen deficiency, including hot flashes, vaginal dryness, and osteoporosis risk. Diagnosis is typically confirmed by elevated follicle-stimulating hormone (FSH $\geq$25 IU/L) and low estradiol (E2) levels on at least two occasions. Biomarkers such as anti-Müllerian hormone (AMH) provide additional insight into ovarian reserve [4, 5]. POI is a heterogeneous disorder with multiple contributing factors, including genetic mutations [6], autoimmune dysfunction [7], iatrogenic damage [8], and environmental exposures.

Considering its profound impact on reproductive health, effective management strategies exist to mitigate complications. Hormone replacement therapy (HRT) is recommended to prevent osteoporosis, cardiovascular disease, and menopausal symptoms. While emerging regenerative approaches, including stem cell therapy, platelet-rich plasma (PRP), and ovarian tissue transplantation are being explored for ovarian function restoration, the outcomes remain limited. Thus, it is vital to exploit novel therapeutics to treat the POI. Approaches to mitigate the augmented T cell-mediated autoimmunity in the periphery and ovarian microenvironment is the one of the promising insights for POI therapy.

While immune checkpoint blockade (ICB) therapy [9] is primarily used to enhance immune responses in cancer, including target T-cell receptors like programmed cell death protein 1 (PD-1), cytotoxic T-lymphocyte-associated protein 4 (CTLA-4) [10, 11] and T cell immunoglobulin mucin 3 (TIM-3) [12, 13]. However, dysregulation of these checkpoints has been implicated in the pathogenesis of multiple autoimmune diseases, including systemic lupus erythematosus (SLE), rheumatoid arthritis (RA), multiple sclerosis (MS), and type 1 diabetes (T1D).

Immune checkpoint molecules such as programmed cell death protein 1 (PD-1), programmed death-ligand 1 (PD-L1), cytotoxic T-lymphocyte-associated antigen 4 (CTLA-4), lymphocyte-activation gene 3 (LAG-3), and T cell immunoreceptor with Ig and ITIM domains (TIGIT) function to suppress excessive immune responses and prevent autoimmunity. However, in many autoimmune diseases, these inhibitory pathways are either functionally impaired or insufficient to control pathological immune activation. Restoring immune checkpoint signaling has emerged as a potential therapeutic strategy to re-establish immune tolerance and prevent autoimmune-mediated tissue damage.

Autoimmune-mediated POI is thought to result from a breakdown in immune self-tolerance, leading to an aberrant immune response against ovarian tissues. In affected individuals, autoreactive T cells and autoantibodies targeting ovarian antigens contribute to follicular depletion and stromal inflammation, ultimately impairing ovarian endocrine and reproductive function [7, 14, 15]. Histological studies of autoimmune POI cases reveal lymphocytic infiltration of the ovarian cortex, further supporting the role of immune-mediated destruction in disease progression [7]. Given the growing recognition of excessive immune activation in POI, targeted immunomodulatory therapies aimed at restoring immune tolerance are being explored. Immune checkpoint agonists, regulatory T cell enhancement, and cytokine blockade strategies may hold promise for preserving ovarian function in autoimmune POI. However, further research is needed to elucidate the precise immune mechanisms underlying POI and to develop targeted interventions that can mitigate ovarian inflammation while preserving fertility.

Various therapeutic approaches have emerged in the field of POI treatment. Currently, bacteria based therapies, cell therapies [16–19] and biomaterials (such as bioproducts and hydrogel [20] and ovarian regenerative patch [21]) have been widely employed in POI management. Recently, with a better understanding of extracellular vesicle (EV) biology [22], increasing studies have focused on developing genetically engineered EVs as a novel therapeutic strategy. Genetically engineered EVs offer several advantages, including excellent biocompatibility, high stability, and targeted delivery of therapeutic agents to specific tissues without triggering immune rejection or unexpected toxicity [23]. While previous studies have demonstrated that cell therapy can ameliorate POI progression through diverse mechanisms [24–26], its clinical application still faces several limitations. Therefore, in this study, we aimed to: identify a scaffold protein suitable for producing bioengineered EVs; genetically construct plasmids for transfection into cells to produce engineered EVs; isolate and characterize EVs expressing PD-L1 and Gal-9, two immune inhibitory ligands; evaluate the impact of PD-L1-Gal-9 EVs on the immune microenvironment and assess their therapeutic potential in alleviating POI progression.

Methods and materials

Cell culture

The HEK-293 T cells were maintained in DMEM (Gibco) with 1% Penicillin–Streptomycin-Gentamicin (Beyotime Biotechnology) and 10% fetal bovine serum (FBS) (Gibco). The primary CD8 + T cells were isolated and subsequently cultured in RPMI 1640 medium with 10% FBS and 1% gentamicin, supplemented with 1 mM sodium pyruvate, 1000 IU/mL interleukin-2 (IL-2).

Clinical samples

Fresh peripheral blood samples were collected from women diagnosed with POI ($n = 8$) and non-POI healthy women (n = 8) from 2020 to 2024 at Obstetrics and Gynecology Hospital of Fudan University. Separation of peripheral blood mononuclear cells (PBMCs) was performed by Human Peripheral Blood Lymphocyte Separation Medium (Beyotime Biotechnology) and analyzed by the flow cytometry [27].

Plasmid design

Synthetic gene fragments encoding PD-L1 and Galectin-9 were obtained from Maipu Biotechnology (Nanjing, China) and subsequently subcloned into a PLV expression vector. Transmembrane domains of CD63, CD81, CD9, and Lamp2b were similarly synthesized by the same provider for vesicle engineering purposes. The GFP fragment, mCherry fragment, HiBiT fragment were synthesized by Maipu Biotechnology (Nanjing, China). The nanoLuc fragment was gifted from the Obstetrics and Gynecology Hospital of Fudan University.

Mice

The Female C57BL/6 and B6 AF1 (6-week-old) were purchased from The Jackson Laboratory and were housed in animal facility of Experimental Animal Center of Fudan University (Shanghai, China). All mice were housed in specific pathogen-free conditions. The studies were conducted based on the guidelines for the use and care of live animals and were approved by the Animal Care and Use Committees of Fudan University. Female B6 AF1 mice were immunized s.c. with 100 IU ZP3 peptide (amino acids 330–342, NSSSSQFQIHGPR, Invitrogen, Thermo Fisher Scientific) emulsified in complete Freund's Adjuvant (CFA, Sigma, Louis, MO, USA). This method was conducted for consecutive 14 days to induce autoimmune POI model, as previous reported [7]. The vivo experiments were conducted according to an animal

protocol that received approval from the Institutional Animal Care and Use Committee of Fudan University. The POI model mice were kept untreated (control group) or injected with PD-L1-Gal-9 EVs (30 mg/kg) or PBS for every two days through the tail vein for 30 days. The AMH levels of POI mice were monitored at 30 days post-treatment, and then the mice were sacrificed for further analysis.

Isolation of primary mouse T cells

T cells were isolated from diverse organs including ovaries, peripheral blood, livers and spleens. Organs were resected from sacrificed mice and be cutted into small pieces and were digested by collagenase type I (Beyotime Biotechnology), followed by isolation by using EasySep™ Mouse T Cell Isolation Kit (STEMCELL).

Sorting PD-1 + T cells

The PD-1 positive cells were sorted by flowcytometry. The human PD-1 + CD8 + T cells sorting was performed from human PBMCs. The buffy coat of POI patients were collected and were used to isolate the PBMCs by Human Peripheral Blood Lymphocyte Separation Medium (Beyotime Biotechnology). The PBMCs were stained by FITC-CD8a (BioLegend 300,916), BV421-CD3 (BioLegend 344,833) and PE-PD-1 (BioLegend 329,905) and were sorted by BD FACSAria III (BD biosciences).

Immunofluorescent assay

For tissues fluorescence experiment, the ovaries tissues were resected and subsequently embedded in paraffin followed by preparing into issue sections. For the immunofluorescent assay, we selected the primary antibody (anti-PD-1 (abcam, ab300425), anti-Tim3 (abcam, ab314089)) and secondary antibodies to detect the PD-1 expression and Tim-3 expression in mice ovaries. The sections were observed under a fluorescence microscope (Zeiss).

Preparation of PD-L1-Gal-9 EVs

Totally 10^6 HEK-293 T (P11) cells were seeded and cultured in T175 flasks (Beyotime Biotechnology). We transfected cells with plasmids using BeyoPEI™ Transfection Reagent (Beyotime Biotechnology) at a reagent: plasmid ratio of 2:1. After 5 h, the medium was replaced with Opti-MEM (Gibco) supplemented with 1% Penicillin–Streptomycin-Gentamicin (Beyotime Biotechnology) and EV-depleted FBS. After 48 h, the conditioned medium was collected and centrifuged at 2000 g for 10 min. The supernatant was then filtered through a 0.22 μm Syringe Filters (Beyotime Biotechnology). Following this, the supernatant was subjected to additional centrifugation at 100,000 g for 60 min to isolate the genetically engineered EVs. The final EVs were resuspended in PBS and stored at − 80 °C in aliquots for further analysis.

Characterization of engineered PD-L1-Gal-9 EVs

The shape of the bioengineered EVs were characterized by using transmission electron microscope (TEM, FEI Tecnai G2 Spirit Twin, Philips). The size distribution of the bioengineered EVs were measured by nanoparticle tracking analysis, (NTA, NanoSight NS300, Malvern). And the markers of engineered EVs including CD63, Alix, Tsg101 and Grp94 were detected by Western blot experiment. The PD-L1 expression and Gal-9 expression in bioengineered EVs were also detected by Western blot.

Western blot

EVs proteins were detected by Bradford Protein Concentration kit (Thermo Fisher Scientific). Since all the detection in this study is EVs surface protein, we did not lysate the EVs. Then, the EVs were added into the SDS–polyacylamide gel electrophoresis gel according to the standard procedure, followed by blotting onto the polyvinylidene difluoride membrane. After the blocking for 1 h at room temperature and incubation with primary antibody at 4 °C overnight, the membrane was incubated with HRP conjugated secondary antibodies and was visualized with enhanced chemiluminescence. EVs markers detection including CD63 (abcam, ab134045), Alix (abcam, ab275377), Tsg101 (abcam, ab133586) and Grp94 (abcam, ab238126). The PD-L1 (abcam, ab205921) and Gal-9 (abcam, ab228686) were used to detect the presenting ability of bioengineered EVs.

Ex vivo inhibition of T cells

PD-1 + CD8 + T cells were sorted and incubated into the 96-well plates with RPMI (10% FBS) at concentration of 10^6 cells/mL in 6-well-plate. The cells were treated with PBS, balnk EVs and PD-L1-Gal-9 EVs for 24 h, separately. We selected the FITC-Annexin V apoptosis detection kit (Beyotime Biotechnology) to analyze the apoptosis of PD-1 + CD8 + T cells via flow cytometry. In addition, primary spleen CD8 + T cells isolated from mice spleen by EasySep™ Mouse CD8 + T Cell Isolation Kit (Stemcell), then were stimulated with IL-2 (1000 IU/mL) plus CD3/CD28 (25uL/mL), followed by treating with engineered PBS, balnk EVs and PD-L1-Gal-9 EVs for a duration of 48 h. We also used the FITC-Annexin V apoptosis detection kit (Beyotime Biotechnology) to analyze the apoptosis of spleen CD8 + T cells via flow cytometry. Meanwhile, the percentages of mice FOXP3 + Treg cells in T cell population was detected with the same treatment procedure (stmulation and EVs treatments) and detected by flow cytometry.

Flow cytometry

Immune cells from organs were digested and purified for further staining as well as flowcytometry analysis. We selected antibodies as below: anti-CD3-BV421, anti-CD4-A488, anti-CD8-PE, anti-Perforin-PE-Cy7, anti-Granzyme A-BV510, anti-PD-1-APC. Cells were fixed and permeabilized by using Fixation/Permeabilization Solution KiT (554,714, BD). Acquisition and compensation were conducted on a MACS Quant flow cytometry (Miltenyi biotec, Germany). The flow cytometry data were analyzed via FlowJo (10.8.1) software.

ELISA assay

The ELISA assay was performed upon the mice serum to detect the level of AMH, FSH and E2 in serum, which are widely acknowledged classic parameters to diagnose POI. Blood samples were collected and stored at −80 °C until further analysis. Prior to use, samples were thawed on ice and centrifuged at 10,000 × g for 10 min at 4 °C to remove debris. 96-well high-binding ELISA plates were coated with antibodies with capture antibodies specific for AMH, FSH, and E2. The wells were washed with PBS containing 0.05% Tween-20 (PBST) and blocked with 5% BSA for 1 h at room temperature. After washing, HRP-conjugated secondary antibodies were added and incubated for 1 h at room temperature. The reaction was developed using TMB substrate, stopped with 2 N H_2SO_4, and absorbance was measured at 450 nm using a microplate reader (BioTek Synergy HT).

Immunoreactivity score

Tissue sections were subjected to immunohistochemical (IHC) staining to detect the expression of Bax and Bcl-2. Staining evaluation was performed using a double-blind method by two independent pathologists. A semiquantitative scoring system was applied based on staining intensity and proportion of positive cells. Staining intensity: 3 = brown, 2 = light brown, 1 = light yellow, and 0 = no color. Proportion of positive cells: 4 = (> 75%), 3 = (51 ~ 75%), 2 = (25 ~ 50%), 1 = (5 ~ 25%), and 0 = (< 5%). The immunoreactivity score was determined as the sum of the intensity and positivity scores. The median MVIS for each experimental group was calculated for statistical analysis.

Statistical analysis

The mean values of the data are presented with standard deviations (SD). The sample size (n) for each statistical analysis is specified in the figure legends, where applicable. All statistical analyses were performed using Prism 10.2.0 (GraphPad Software). Biological replicates were used in all studies unless otherwise stated. For comparisons involving multiple groups, one-way analysis of variance (ANOVA) was performed. P-value < 0.05 was considered statistically significant.

Results

Dysregulated T cells distribution in POI

To assess immune dysregulation in primary ovarian insufficiency, peripheral T cell subpopulations in POI patients (N = 8) and healthy controls (N = 8) were detected using flow cytometry. POI patients exhibited a significantly increased percentage of PD-1 expression in CD8+ T cells (Fig. 1A) as well as the increased percentage of CD8+ T cells in CD3+ T cells (Fig. 1B) compared to controls. Next, we examined ovarian infiltrating T cell subpopulations in POI mice (N = 8) and control mice (N = 8). Similarly, POI mice showed a significantly higher percentage of CD8 + T cells (Fig. 1D) and PD-1 + CD8 + T cells (Fig. 1E) in the ovaries. In addition, the percentage of Foxp3+ Treg cells exhibited a reduced proportion in both patients' samples (Fig. 1C) and mice model (Fig. 1F).

Identification of diverse EVs for presenting molecules

We genetically engineered the EVs with different scaffold protein to produce the EVs as below: CD63-HiBiT EVs, CD81-HiBiT EVs, CD9-HiBiT EVs and Lamp2b-HiBiT EVs. Then, we compared the loading ability of HiBiT into the engineered EVs by HiBiT Protein Tagging System.

According to the results from Fig. 2B, the Lamp2b could load more HiBiT Protein than other scaffold proteins. Similarly, according to the results from Fig. 2C, the Lamp2b-loaded EVs treated PBMCs could exhibit higher bioluminescence signaling than other scaffold proteins-loaded EVs treated PBMCs. To conclude, Lamp2b was selected as the scaffold to produce the EVs to present the proteins of interests. Then, we produced the bioengineered EVs from HEK-293 T cells (Fig. 2A), we observed the characteristics of bioengineered EVs by transmission electron microscopy (TEM) and evaluate the size distribution by NTA. Bioengineered EVs exhibited typically spherical or cup-shaped (Fig. 2D) and ranged from 40 to 300 nm (Fig. 2E). Meanwhile, the bioengineered EVs exhibited expression of CD63, Aix and Tsg101 (Fig. 2F, Supplementary S1), which are classic EVs markers.

The binding ability of PD-L1-Gal-9 EVs produced by "all in one" plasmid strategy

We compared the binding ability of EVs produced with different transfection strategies. We transfected the HEK-293 T cells with plasmids as below to produce EVs: "PD-L1-Lamp2b-nanoLuc", "Gal9-Lamp2b-nanoLuc", "PD-L1-Lamp2b-nanoLuc-P2A-Gal9-Lamp2b-nanoLuc". Then we treated the T cells with these EVs separately at equal number of particles and detected the

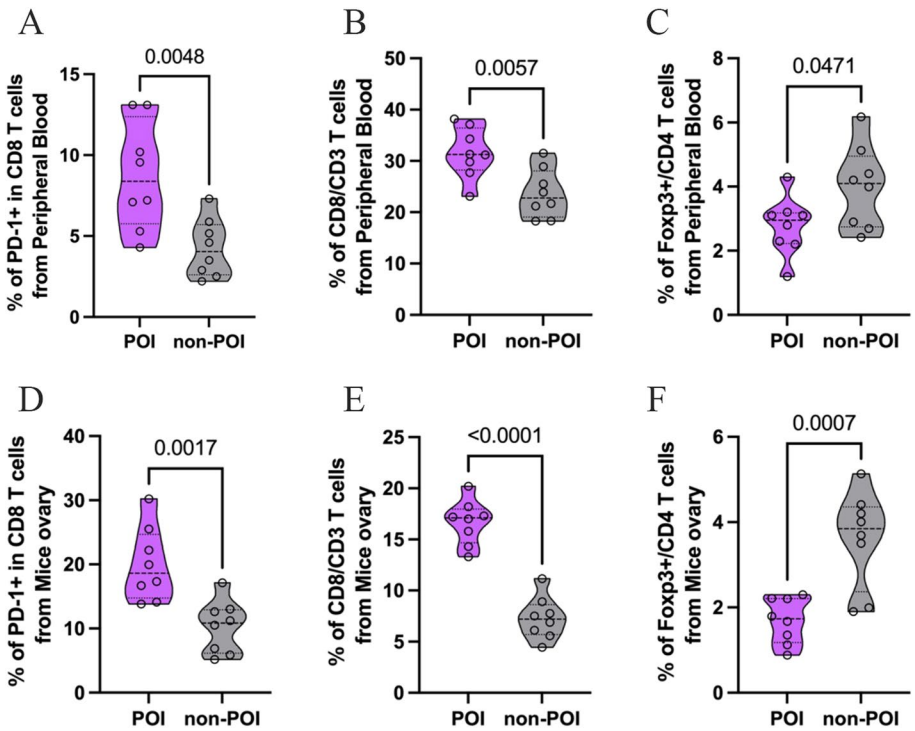

Fig. 1 Dysregulated T cells distribution in POI. **A** The percentage of PD-1 +T cells in periphery patients with POI ($n = 8$) and control ($n = 8$). **B** The percentage of CD8 +T cells in periphery patients with POI ($n = 8$) and control ($n = 8$). **C** The percentage of Foxp3 +T cells in periphery patients with POI ($n = 8$) and control ($n = 8$). **D** The percentage of PD-1 +T cells in ovaries from POI mice ($n = 8$) and control ($n = 8$). **E** The percentage of CD8 +T cells in ovaries from POI mice ($n = 8$) and control ($n = 8$). **F** The percentage of Foxp3 +T cells in ovaries from POI mice ($n = 8$) and control ($n = 8$)

bioluminescence signaling of EVs as well as EVs treated T cells (Fig. 3B). As depicted in Fig. 3C, the PD-L1-Lamp2b-nanoLuc EVs showed similar bioluminescence signal to Gal9-Lamp2b-nanoLuc EVs and PD-L1-Lamp2b-nanoLuc-P2A-Gal9-Lamp2b-nanoLuc EVs. However, the cells treated with EVs produced by "PD-L1-Lamp2b-nanoLuc-P2A-Gal9-Lamp2b-nanoLuc" exhibited higher bioluminescence signal than other groups (Fig. 3D). This result indicated that it is feasible to produce the EVs by "all in one" plasmid, which could exhibit better binding ability. Meanwhile, we also transfected the HEK-293 T cells with plasmids as below to produce EVs as below: "PD-L1-GFP-Lamp2b", "Gal9-mCherry-Lamp2b", "PD-L1-GFP-Lamp2b-P2 A-Gal9-mCherry-Lamp2b". Then we treated the T cells with these EVs separately at equal number of particles (Fig. 3A). As depicted in Fig. 3E, the cells treated with EVs produced by "PD-L1-GFP-Lamp2b-P2 A-Gal9-mCherry-Lamp2b" exhibited both GFP expression and mCherry expression, while cells treated with EVs produced by "PD-L1-GFP-Lamp2b" only exhibited GFP expression (Fig. 3F), and cells treated with EVs produced by "Gal9-mCherry-Lamp2b" only exhibited mCherry expression (Fig. 3G). In addition, the PD-L1-GFP-Gal-9-mCherry EVs expressed the PD-L1 and the Gal-9 (Fig. 3H, Figure S2), while the PD-L1-GFP EVs expressed PD-L1 and Gal-9-mCherry EVs expressed Gal-9. Above all, these results indicated that the "all in one" plasmid strategy is feasible to produce EVs to present molecules, and PD-L1-Gal-9 EVs exhibited effective ability to bind to the T cells.

The biological behavior of PD-L1-Gal-9 EVs with PD-1 +T cells and pan-T cells ex vivo

To detect the biological behavior of engineered PD-L1-Gal-9 EVs on the PD-1 positive T cells, we sorted the PD-1 positive T cells and Tim-3 positive T cells from PBMCs (Fig. 4A), followed by treating with PD-L1-Gal-9 EVs to evaluate the apoptosis of these cells. As depicted in Fig. 4C and D, the PD-L1-Gal-9 EVs could promote the apoptosis of PD-1 positive T cells significantly. We also isolated the primary T cells from mice spleen (Fig. 4B) and stimulated them followed by treating with PD-L1-Gal-9 EVs. As demonstrated in Fig. 4E and F, the engineered PD-L1-Gal-9 EVs could promote the apoptosis in primary mouse T cells. What's more, the Foxp3 expression in primary mouse T cells decreased after treated with PD-L1-Gal-9 EVs (Fig. 4G and H).

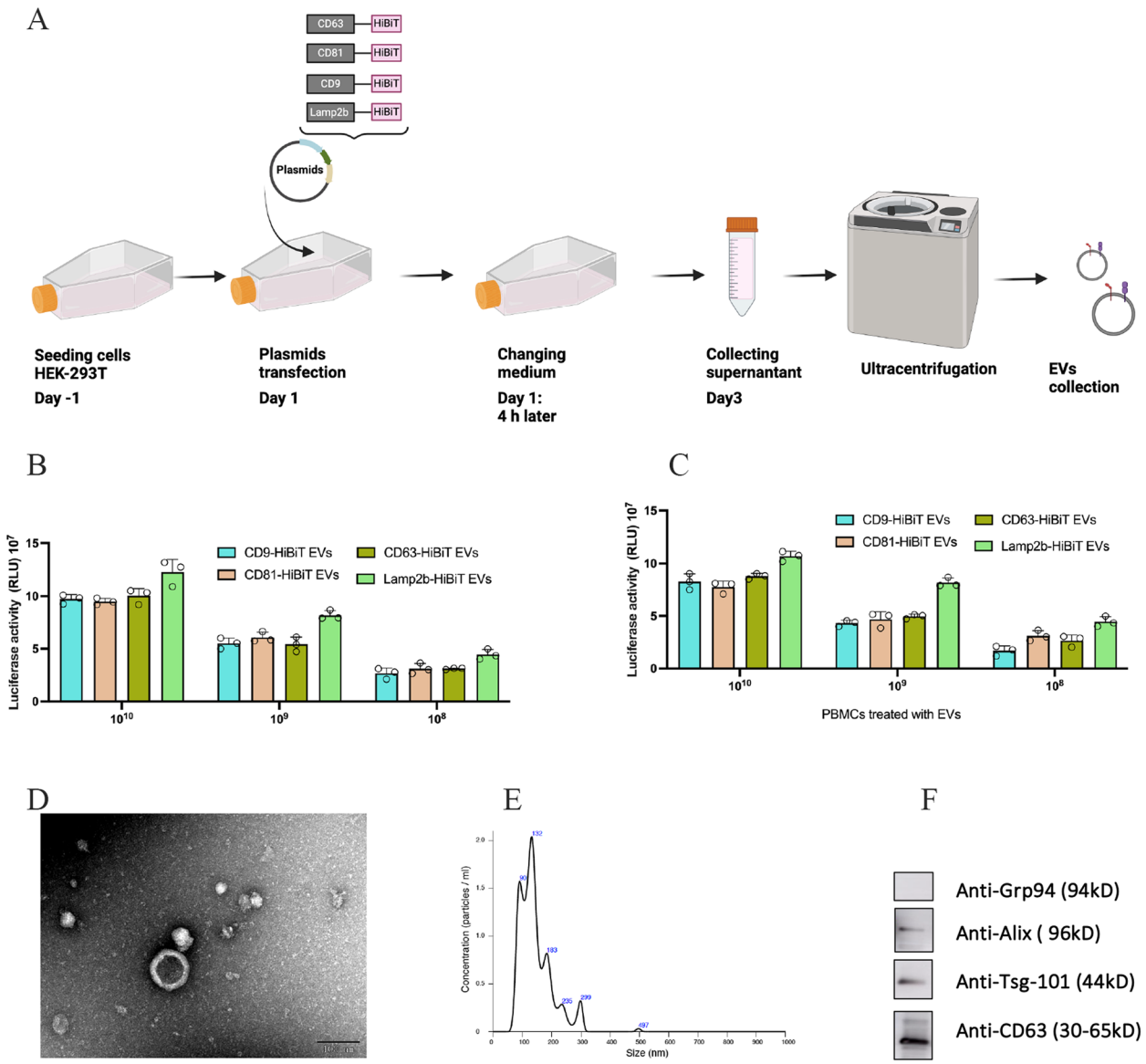

Fig. 2 Identification the scaffold for engineering EVs. **A** The cartoon diagram of detailed procedure for engineering EVs to present PD-L1 and Gal-9. **B** The bioluminescence signal of bioengineered EVs produced by different strategies. **C** The bioluminescence signal of different bioengineered EVs treated T cells. **D** The TEM images of bioengineered EVs (Bar: 100 nm). **E** The size distribution of bioengineered EVs. **F** The surface markers detection of bioengineered EVs

(See figure on next page.)

Fig. 3 The analysis of effective binding and uptake of PD-L1-Gal-9 EVs in T cells. **A** The cartoon diagram of evaluating the binding ability of bioengineered EVs (expressing PD-L1-GFP and Gal-9-mCherry). **B** The cartoon diagram of evaluating the binding ability of bioengineered EVs (expressing PD-L1-nanoLuc and Gal-9-nanoLuc). **C** The bioluminescence signal of bioengineered EVs produced by different strategies. **D** The bioluminescence signal of different bioengineered EVs treated T cells. **E** The fluorescence of T cells treated with bioengineered EVs produced by different strategies. **F** The statistical image of GFP expression in T cells treated with bioengineered EVs produced by different strategies. **G** The statistical image of mCherry expression in T cells treated with bioengineered EVs produced by different strategies. **H** The expression of PD-L1 and Gal-9 in bioengineered EVs produced by different strategies

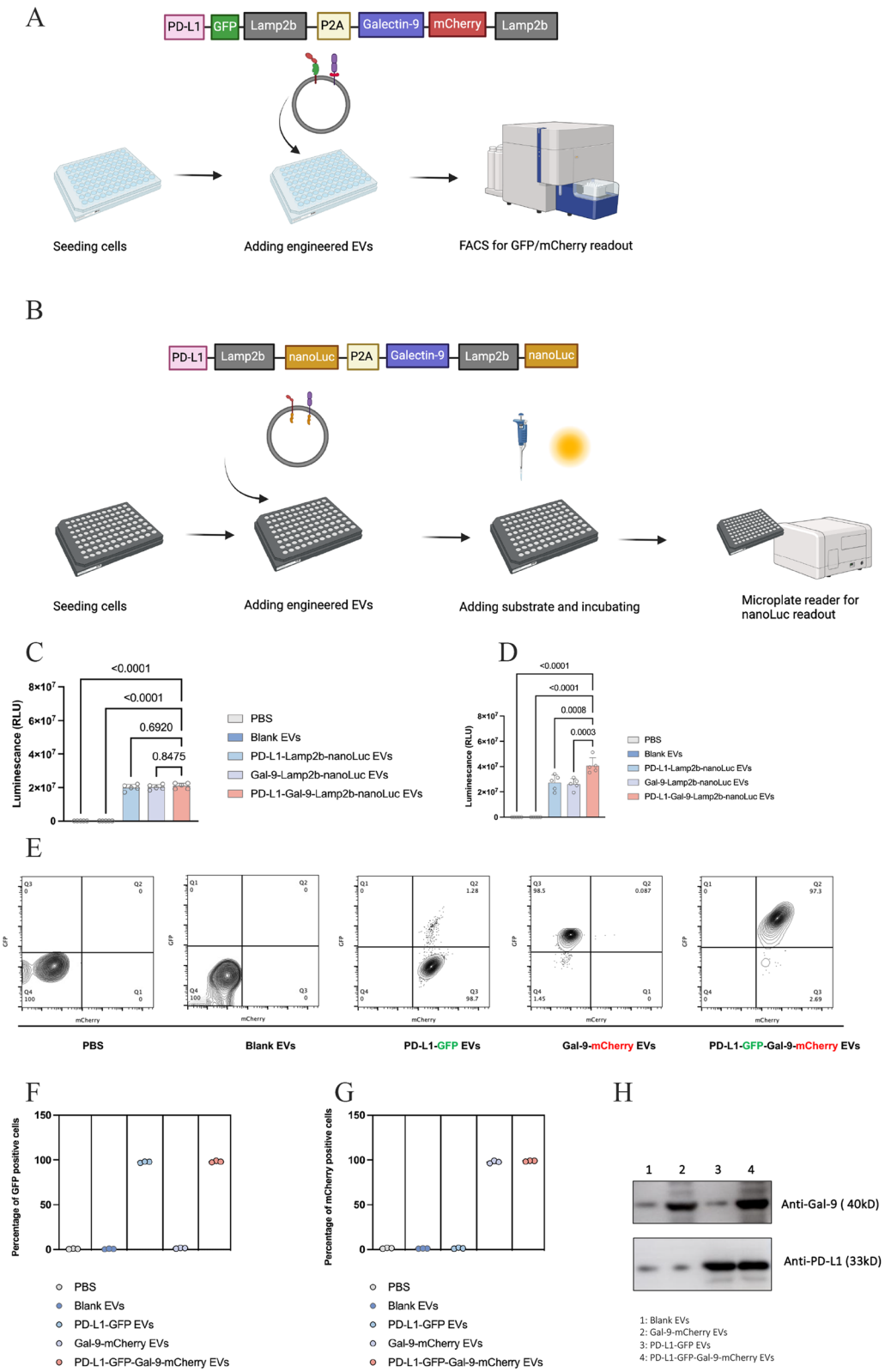

Fig. 3 (See legend on previous page.)

Therapeutic efficacy of PD-L1-Gal-9 EVs in POI mice

To further evaluate the therapeutic potential of PD-L1-Gal-9 EVs in POI progression in vivo, a POI mouse model was established using pZP3, as previously reported [28–30]. As shown in Fig. 5B and C, treatment with bioengineered PD-L1-Gal-9 EVs significantly restored ovarian volume and weight in POI mice to near-normal levels, with no significant loss of body weight. Additionally, the numbers of preovulatory, secondary, primary, and primordial follicles were reduced in the POI group, but this reduction was reversed following PD-L1-Gal-9 EVs treatment (Fig. 5E and F). Furthermore, administration of genetically bioengineered PD-L1-Gal-9 EVs restored the decreased levels of estradiol (E2) (Fig. 5G) and anti-Müllerian hormone (AMH) (Fig. 5I) in POI mice. Meanwhile, the elevated follicle-stimulating hormone (FSH) levels in POI mice were also reversed upon treatment (Fig. 5H).

Bioengineered PD-L1-Gal-9 EVs could suppress the over-activated T cells in POI mice

Ovaries were collected from POI mice subjected to various treatments, followed by immunofluorescence analysis to detect PD-1 and TIM-3 expression. In untreated mice with normal AMH levels, PD-1 + cells and TIM-3 + cells were almost absent in the ovaries. In contrast, POI mice exhibited notable infiltration of PD-1 + and TIM-3 + cells within the ovaries (Fig. 6A), indicating that immune-toxic T cell infiltration contributes to ovarian cell destruction in POI. Meanwhile, genetically bioengineered PD-L1-Gal-9 EVs could decrease the infiltration of PD-1 + and TIM-3 + cells. According to the immunoactivity score, PD-L1-Gal-9 EVs could result in the low apoptosis effect of ovaries (Fig. 6B and C). Encouragingly, flow cytometry analysis further confirmed that treatment with genetically bioengineered PD-L1-Gal-9 EVs partially reduced the proportion of PD-1 + T cells (Fig. 6D and E) as well as TIM-3 + T cells (Fig. 6F and G) compared to the PBS-treated POI group. It is well established that ovarian cells are eliminated by activated CD8 + cytotoxic T lymphocytes (CTLs) via cytokine secretion, including Granzyme A and perforin. To evaluate the involvement of these cytotoxic mechanisms, we assessed the proportion of $CD8^+$ T cells expressing perforin and Granzyme A within the ovaries. Flow cytometry results revealed a significant increase in perforin + CD8 + T cells (Fig. 6H and I) and Granzyme A + CD8 + T cells (Fig. 6J and K) in POI mice. Collectively, these data indicate that PD-L1-Gal-9 EVs effectively suppress infiltrating CD8 + T cell activity within the ovaries, contributing to the restoration of ovarian function in POI mice.

Biodistribution evaluation of bioengineered EVs

To evaluate the pharmacokinetics, and biodistribution of the bioengineered EVs in POI mice, we genetically fused an NanoLuc to the EVs (PD-L1-Gal-9-Lamp2b-nanoLuc EVs). This modification allows the EVs to generate a bright bioluminescent signal when bound to substrate [31]. Following the production of PD-L1-Gal-9-Lamp2b-nanoLuc EVs, the engineered EVs were administered to POI mice via intravenous injection at a standardized time point (Fig. 7A). Mice were then sacrificed at 1 day, 3 days, 7 days and 14 days to evaluate bioluminescent signal intensity and lymphocyte composition across different organs. As shown in Fig. 7B, high bioluminescent signals were detected in all organs at 1-day post-injection. By 3 days, more than 50% of the bioluminescent signal had diminished across all organs, including peripheral blood. After 3 and 7 days, minimal residual signals were detected with all the organs. Furthermore, after PD-L1-Gal-9-Lamp2b-nanoLuc EVs, we observed a decreased percentage of CD8 + T cells in the ovaries at 3 days post-injection (Fig. 7D). However, the level of $CD8^+$ T cell percentages kept stable after 3 days post-injection. Additionally, at 3 days post-injection, we detected a reduction in perforin + CD8 + T cells (Fig. 7C) and Granzyme A + CD8 + T cells (Fig. 7E) in the organs and peripheral blood, which kept stable level at 7 days post-injection. Collectively, these data indicated that PD-L1-Gal-9 EVs only exhibited short-term inhibition of over-activated cytotoxicity CD8 + T cells and limited long-term distribution in POI mice.

Discussion

Primary Ovarian Insufficiency (POI) is a complex disorder characterized by premature ovarian dysfunction, often leading to infertility and other systemic complications [2]. Emerging evidence suggests that autoimmune mechanisms play a critical role in the pathogenesis of POI, with autoantibodies targeting ovarian tissue and immune dysregulation contributing to follicular

(See figure on next page.)

Fig. 4 The effect of PD-L1-Gal-9 EVs on PD-1 + T cells and primary spleen T cells ex vivo. **A** The cartoon diagram of detecting the effect of bioengineered PD-L1-Gal-9 EVs on sorted PD-1 positive T cells. **B** The cartoon diagram of detecting the effect of bioengineered PD-L1-Gal-9 EVs on primary mice spleen T cells. **C** The apoptotic effect of bioengineered PD-L1-Gal-9 EVs on the PD-1 positive T cells ex vivo ($n = 3$). **D** Statistical diagram for (**C**). **E** The apoptotic effect of bioengineered PD-L1-Gal-9 EVs on the primary mice spleen T cells ex vivo ($n = 3$). **F** Statistical diagram for (**E**). **G** The regulating effect of bioengineered PD-L1-Gal-9 EVs on Treg cells generation ex vivo ($n = 3$). **H** Statistical diagram for (**G**)

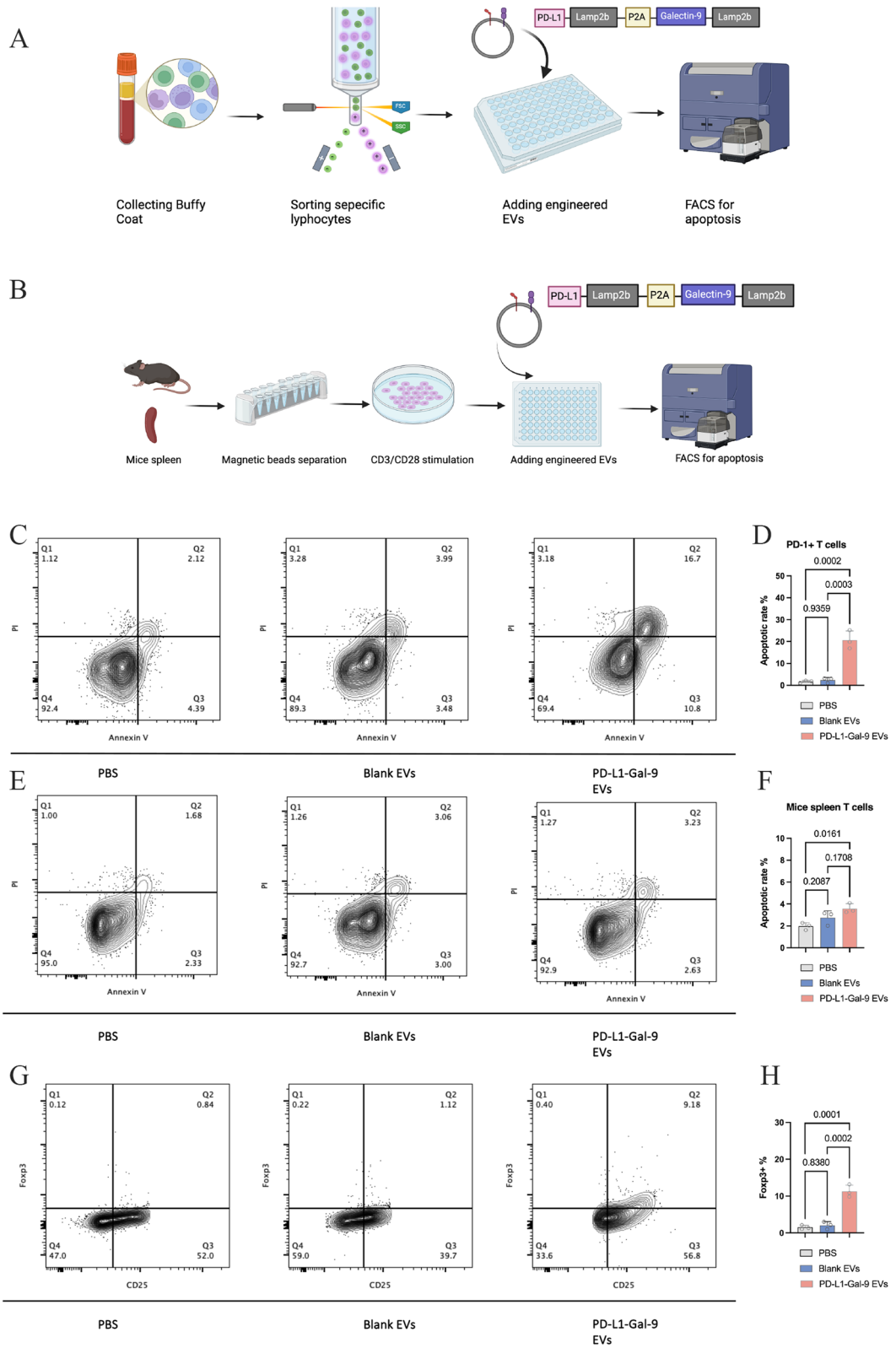

Fig. 4 (See legend on previous page.)

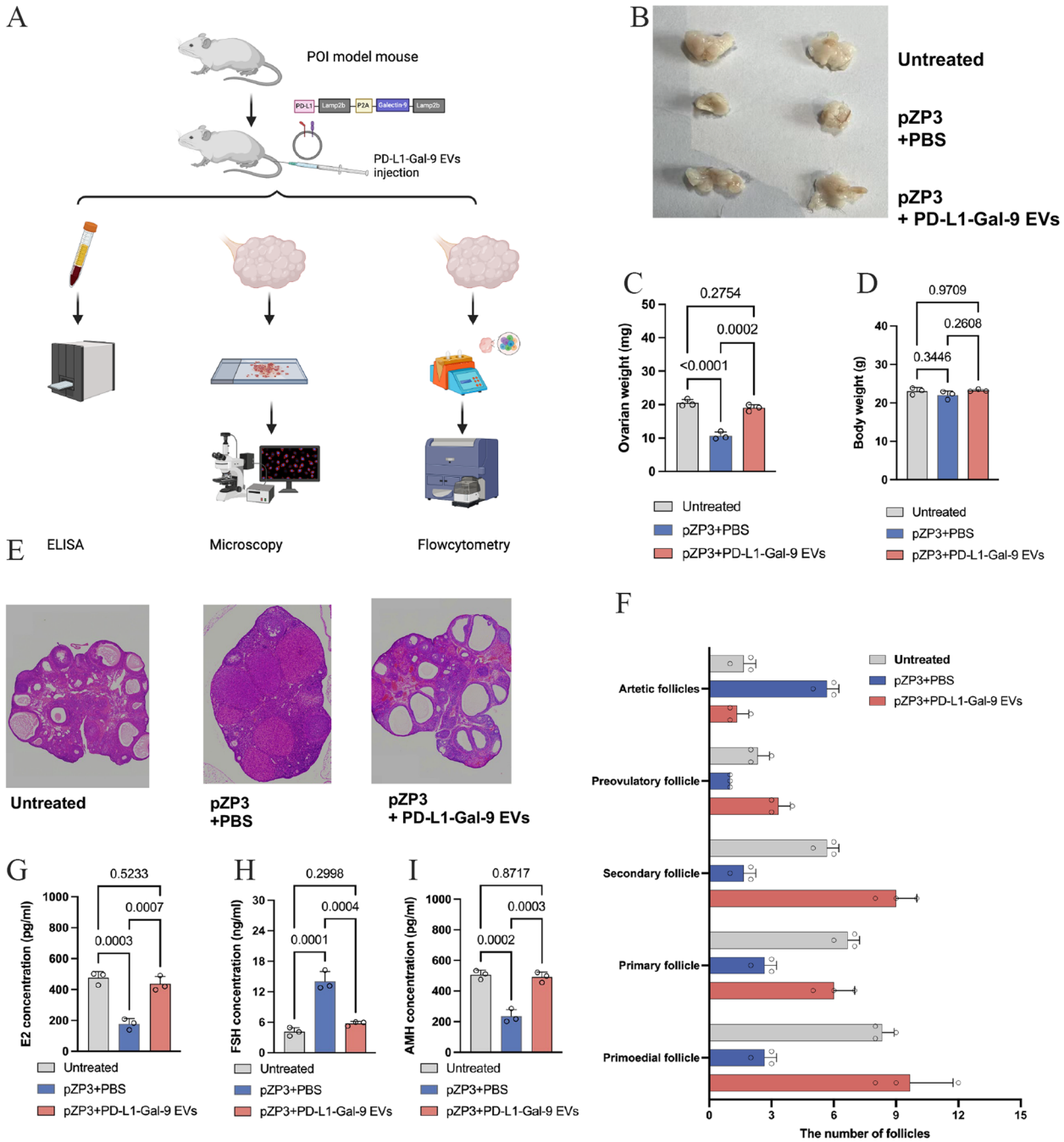

Fig. 5 The therapeutic effect of PD-L1-Gal-9 EVs in POI mice. **A** The cartoon diagram of evaluating the therapeutic effect of bioengineered PD-L1-Gal-9 EVs in POI mice. **B** Image of Gross ovaries from Untreated ($n = 3$), pZP3 + PBS ($n = 3$) and pZP3 + PD-L1-Gal-9 EVs ($n = 3$) treated mice. **C** The weights of ovaries from mice with diverse treatments ($n = 3$). **D** The body weights of mice with diverse treatments ($n = 3$). **E** The images of ovaries' HE staining from mice with diverse treatments. **F** The number of follicles at different stages from mice with diverse treatments based on the HE staining ($n = 3$). **G** The E2 level in mice with diverse treatments ($n = 3$). **H** The FSH level in mice with diverse treatments ($n = 3$). **I** The AMH level in mice with diverse treatments ($n = 3$)

depletion. Given this understanding, therapeutic strategies aimed at modulating the autoimmune response have gained interest as potential treatments for POI.

In our study, we explored the efficacy of immunomodulatory interventions in mitigating ovarian damage and preserving ovarian function by genetically bioengineered

extracellular vesicles. Firstly, we compared the ability of four published EVs scaffold proteins in producing EVs and identified the "Lamp2b" as the scaffold protein in our study. Then we compared different producing strategies in HEK-293 T cells, including PD-L1-Lamp2b EVs, Gal-9-Lamp2b EVs and PD-L1-Gal-9-Lamp2b EVs, and found that the PD-L1-Gal-9-Lamp2b EVs exhibited better binding ability than other two EVs. Then, we produced bioengineered EVs to presenting PD-L1 and Gal-9. The engineered PD-L1-Gal-9 EVs could promote apoptosis in primary human CD8 + PD-1 + T cells ex vivo. Also, the PD-L1-Gal-9 EVs could promote apoptosis in primary mouse spleen T cells. These results are consistence to previous studies [32, 33]. Based on the excellent performance to induce apoptosis of overactivated effector T cells, the genetically bioengineered engineered PD-L1-Gal-9 EVs exhibit ability to increase the AMH levels and subsequent ability to preserve the ovarian function. Consequently, the engineered EVs presenting PD-L1 and Gal-9 could bind to "overactivated T cells" and induce them apoptosis, which results in the postpone of POI progression.

In this study, we selected the HEK-293 T cells to produce the EVs. While increasing studies have reported that both MSCs and MSCs-EVs [34, 35] could exhibit promising ability in suppressing inflammation as well as wound healing. However, considering the availability of MSCs as well as the transfection efficacy of MSCs, we selected the HEK-293 T cells as the producing cells for POI therapy. Some previous studies reported that MSCs based therapies could delay the progression of POI [18, 36] by suppressing inflammation, promoting tissue remodeling, and regulating the immune system [18, 37, 38]. However, MSCs therapies remain limited in the clinical practice. HEK-293 T cells are a promising alternative as cell origin in the therapy fields. Furthermore, considering the critical roles of cell therapies in POI therapy field, we selected engineered extracellular vesicles presenting Gal-9 and PD-L1 as a novelty therapeutic platform.

Extracellular vesicles are nanoscale membrane-bound vesicles secreted by cells that play a crucial role in cell-to-cell communication by transferring bioactive molecules, including proteins, lipids, and nucleic acids (mRNAs, microRNAs, and lncRNAs) [39–42]. In recent years, bioengineered extracellular vesicles have emerged as a promising tool for modulating the immune microenvironment, offering potential therapeutic strategies for autoimmune diseases [43], cancer, and tissue regeneration. While increasing MSCs derived engineered EVs are widely studied and exert potential immune regulation ability [44]. However, the strict procedure of culturing MSCs and the subsequent increased cost of producing MSC-derived EVs limit the widely use in clinical practice. Here, we explored the HEK-293 T derived genetically bioengineered EVs could make the procedure economic-effective and promote the widely application. Here, we enrolled and compared four classic EVs sorting domains [45], including CD63 [46, 47], CD9 [48], CD81 and Lamp2b [49, 50] to fuse the proteins of interests outside the EVs membrane, the results showed that the Lamp2b performed better than other three scaffold proteins. Lamp2b, with full name as lysosome-associated membrane protein 2b, is a transmembrane protein that is naturally enriched on the surface of EVs. Lamp2b serves as a stable scaffold for surface engineering, allowing for the display of targeting ligands, peptides, or antibodies. Our result indicated that Lamp2b-based engineering could provide a powerful strategy to enhance the therapeutic efficacy of EVs.

While researchers need to transfect several plasmids into the producing cells for different molecules presenting in previous reported studies. It is a remarkable improvement to use the "all in one" plasmid strategy to produce the bioengineered EVs. In this study, we used P2 A [51] link the "PD-L1-Lamp2b-nanoLuc" and "Gal-9-Lamp2b-nanoLuc", the result showed that there is no significant difference of "nanoLuc" payload of different strategy. However, the "all in one" strategy EVs could exhibit higher bioluminescence signal. It might because of that the co-expression of PD-L1 and Gal-9 could help the bioengineered EVs acquire higher binding ability. The result indicated the feasibility and its effective of "all in one" plasmid strategy to produce bioengineered EVs.

The POI model was used the same method reported in other published studies [29, 30]. The zona pellucida 3 (ZP3)-induced Primary Ovarian Insufficiency (POI) model is based on the principle of autoimmune-mediated ovarian failure, which mimics the mechanisms

(See figure on next page.)

Fig. 6 Bioengineered PD-L1-Gal-9 EVs suppress the over-activated T cells in POI mice. **A** Representative images of PD-1 and TIM-3 expression in ovarian sections. **B** The immunoreactivity score of Bcl-2 of ovaries from mice subjected to different treatments ($n = 3$). **C** The immunoreactivity score of Bax of ovaries from mice subjected to different treatments ($n = 3$). **D** Representative plots illustrating PD-1 + CD8 + T cells within the ovaries of mice subjected to different treatments ($n = 3$). **E** Statistical images for (**D**). **F** Representative plots illustrating PD-1 + TIM-3 + T cells within the ovaries of mice subjected to different treatments ($n = 3$). **G** Statistical images for (**F**). **H** Representative plots illustrating perforin + CD8 + T cells within the ovaries of mice subjected to different treatments ($n = 3$). **I** Statistical images for (**H**). **J** Representative plots illustrating Granzyme A + CD8 + T cells within the ovaries of mice subjected to different treatments ($n = 3$). **K** Statistical images for (**J**)

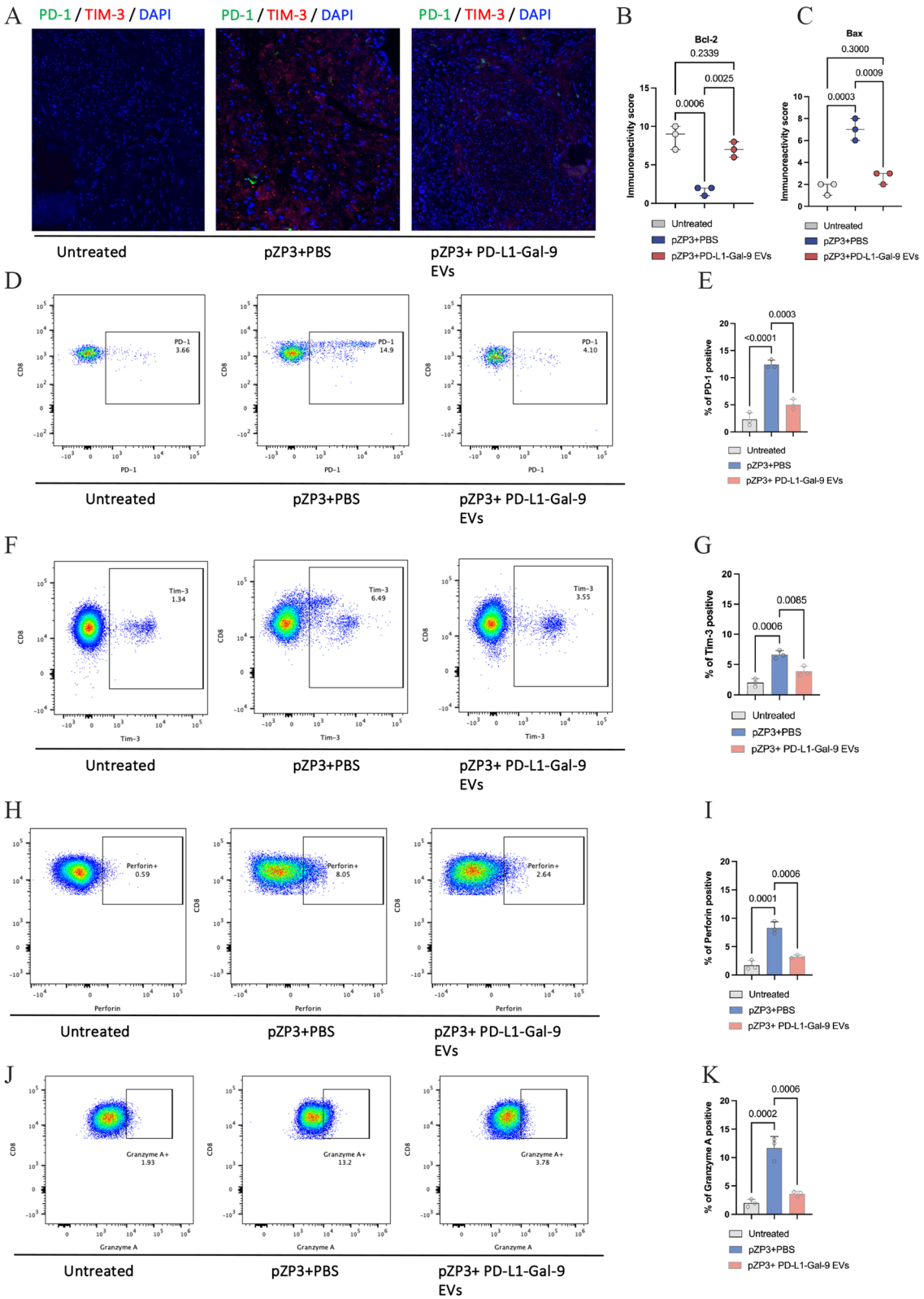

Fig. 6 (See legend on previous page.)

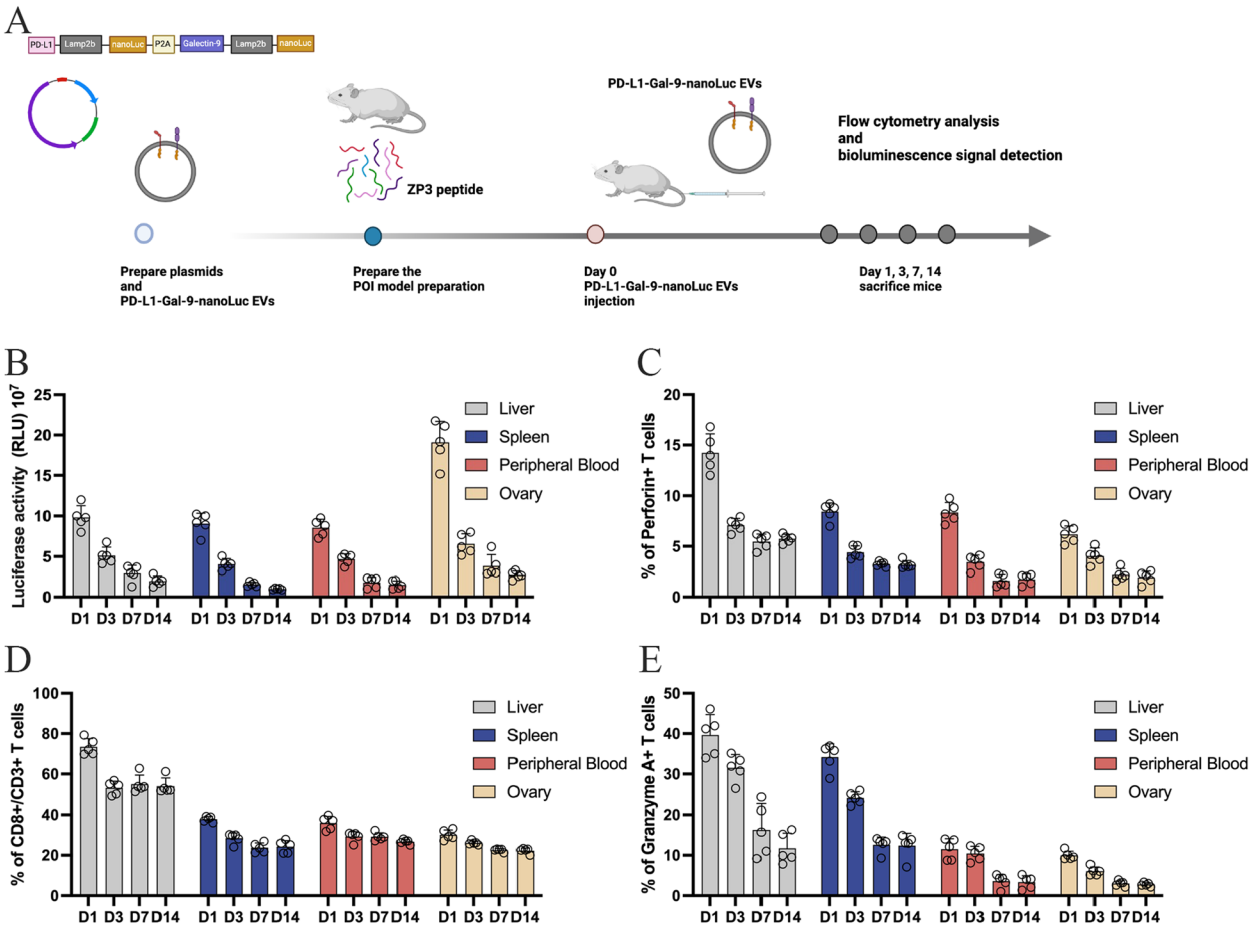

Fig. 7 Biodistribution evaluation of bioengineered EVs. **A** The cartoon diagram of distribution evaluation of bioengineered EVs in POI mice. **B** Statistical image of bioluminescent signal at different post injection timepoints of different organs in POI mice ($n = 5$). **C** Statistical image of perforin + CD8 +T percentage at different post injection timepoints of different organs in POI mice ($n = 5$). **D** Statistical image of CD8 +T cells percentage at different post injection timepoints of different organs in POI mice ($n = 5$). **E** Statistical image of Granzyme A + CD8 +T percentage at different post injection timepoints of different organs in POI mice ($n = 5$)

underlying immune-related POI in humans. The pZP3 protein, a glycoprotein component of the ovarian zona pellucida, serves as an autoantigen, triggering an autoimmune response against ovarian tissue when introduced into an immunized host. When ZP3 is introduced as an antigen, it triggers an autoimmune response, leading to the production of autoantibodies and autoreactive T cells targeting ovarian follicles. This process closely resembles immune-mediated ovarian failure observed in autoimmune-related POI in humans. The ZP3-induced POI model effectively replicates the immune-mediated mechanisms of POI, making it a valuable tool for testing immunomodulatory therapies designed to counteract ovarian autoimmunity and restore reproductive function.

While immune checkpoint blockade (ICB) therapy is primarily used to enhance immune responses in cancer treatment [52–54], a different approach is required for autoimmune diseases, where the immune system is overactive and mistakenly attacks self-tissues. In this context, immune checkpoint agonists (stimulatory therapy) or checkpoint-enhancing strategies can be used to restore immune tolerance and suppress autoimmunity. Immune checkpoint pathways, including programmed cell death protein 1 (PD-1)/programmed death-ligand 1 (PD-L1) [55, 56] and cytotoxic T-lymphocyte-associated antigen 4 (CTLA-4), play a fundamental role in maintaining immune tolerance and preventing excessive immune activation [57]. Dysregulation of these checkpoints has been implicated in multiple autoimmune diseases, including systemic lupus erythematosus (SLE), rheumatoid arthritis (RA), and type 1 diabetes (T1D) [39, 58, 59], and may also contribute to the pathogenesis of POI. Defects in regulatory T cell (Treg) function, which normally suppress autoreactive immune responses, have also been observed in autoimmune POI, further exacerbating ovarian inflammation.

As for the long-term persistence of engineered EVs in vivo and its potential suppression upon the immune system, we conducted the animal assay to evaluate the biodistribution of EVs encapsulated "nanoLuc" by bioluminescence signal at different timepoints. The bioluminescence signal decreased after the bioengineered EVs injection for 3 days and almost disappeared after the bioengineered EVs injection for 7 days. This result trend is similar in live, spleen, ovary and peripheral blood. Based on our results, it showed that the bioengineered EVs could be clearance with several days post injection. As for the potential suppression upon immune system, we detect the percentage of lymphocytes in different organs, the results showed that the bioengineered EVs could inhibit the overactivated perforin + CD8 + T cells as well as Granzyme A + CD8 + T in live, spleen, ovary and peripheral blood. However, the bioengineered EVs exhibited insignificant of CD8 + T cells percentage at 3 days post-injection, which indicated that the effect of bioengineered EVs in suppressing immune system is insignificant.

There are also several limitations of this study. Firstly, engineered EVs should be compared with the soluble antibodies in vitro and in vivo. Secondly, whether the engineered EVs could influence the function of the bone marrow derived cells need to be evaluated. Nonetheless, considering the various advantages of EVs, the engineered EVs are considered potential candidates for disease therapies.

This study significantly broadens the potential applications of genetically bioengineered EVs, which means they could simultaneously present specific ligands on their surface to interact with immune cells. Moreover, the strategic design of these EVs effectively mitigates POI progression in a mouse model by inducing apoptosis in autoreactive T cells, thereby protecting ovarian cells from autoimmune-mediated damage. This innovative approach holds great promise for both alleviating and slowing the progression of POI.

Supplementary Information

The online version contains supplementary material available at https://doi.org/10.1186/s12964-025-02226-8.

Supplementary Figure S1. The expression of markers in PD-L1-Gal-9 EVs. The original membrane of CD63, Tsg101, Alix and GRP94 expression in PD-L1-Gal-9 EVs through Western blot detection

Supplementary Figure S2. The expression of engineered molecules in diverse EVs. The original membrane of PD-L1 and Gal-9 expression in blank EVs, PD-L1 EVs, Gal-9 EVs and PD-L1-Gal-9 EVs through Western blot

Supplementary Figure S3. The gating strategy to sort the PD-1 positive cells. The sorting strategy for collecting the CD8+PD-1+ T cells from the PBMCs

Supplementary Material 4

Supplementary Material 5

Acknowledgements
We gratefully thank all colleagues in the Shanghai Key Laboratory of Female Reproductive Endocrine Related Diseases. This study was supported by the Project of National Natural Science Foundation of China (No.32060208, No.82260532), General program of Guangxi Natural Science Foundation (No.2019 JJA140071).

Authors' contributions
G.N.Z. and Y.Y.G. conceived and performed experiments, wrote the manuscript. M.L.Z., F.S. and J.X.D. collected the samples and analyzed the data. G.M.L. provided reagents. K.Q.H., F.S. and G.N.Z. provided supervision.

Funding
This study was supported by the Project of National Natural Science Foundation of China (No.81771524, No.81471416, No.32060208, No.82260532), General program of Guangxi Natural Science Foundation (No.2019 JJA140071).

Data availability
No datasets were generated or analysed during the current study.

Declarations

Ethics approval and consent to participate
All animal procedures were performed in accordance with the protocol approved by the Institutional Animal Care and Use Committee at the Fudan University (SYXK2020-0032).

Consent for publication
Not applicable.

Competing interests
The authors declare no competing interests.

Author details
[1]Department of Gynecology, The Obstetrics and Gynecology Hospital of Fudan University, 419 Fang-Xie Road, Shanghai 200011, People's Republic of China. [2]Shanghai Key Laboratory of Female Reproductive Endocrine Related Diseases, Shanghai 200011, China. [3]Department of Breast and Thyroid Surgery, Affiliated Hospital of Youjiang Medical University for Nationalities, Baise, China. [4]Key Laboratory of Molecular Pathology in Tumors of Guangxi, Baise, Guangxi 533000, China.

Received: 3 August 2024 Accepted: 30 April 2025
Published online: 28 May 2025

References

1. van Zwol-Janssens C, Pastoor H, Laven JSE, Louwers YV, Jiskoot G. Sexual function in women with premature ovarian insufficiency (POI): systematic review and meta-analysis. Maturitas. 2024;184: 107994.
2. Ding Y, Shao JL, Li JW, Zhang Y, Hong KH, Hua KQ, Wang X. Successful fertility following optimized perfusion and cryopreservation of whole ovary and allotransplantation in a premature ovarian insufficiency rat model. J Ovarian Res. 2018;11(1):35.
3. Memi E, Pavli P, Papagianni M, Vrachnis N, Mastorakos G: Diagnostic and therapeutic use of oral micronized progesterone in endocrinology. Rev Endocr Metab Disord. 2024;25(4):751–772.
4. Xu YP, Fu JC, Hong ZL, Zeng DF, Guo CQ, Li P, Wu JX. Psychological stressors involved in the pathogenesis of premature ovarian insufficiency and potential intervention measures. Gynecol Endocrinol. 2024;40(1): 2360085.
5. Yatsenko SA, Witchel SF, Gordon CM. Primary amenorrhea and premature ovarian insufficiency. Endocrinol Metab Clin North Am. 2024;53(2):293–305.
6. Huang C, Zhao S, Yang Y, Guo T, Ke H, Mi X, Qin Y, Chen ZJ, Zhao S: TP63 gain-of-function mutations cause premature ovarian insufficiency by inducing oocyte apoptosis. 2023;133(5):e162315.
7. Jiao X, Zhang X, Li N, Zhang D, Zhao S, Dang Y, Zanvit P, Jin W, Chen ZJ, Chen W, et al. T(reg) deficiency-mediated T(H) 1 response causes human

premature ovarian insufficiency through apoptosis and steroidogenesis dysfunction of granulosa cells. Clin Transl Med. 2021;11(6): e448.
8. Wang F, Liu Y, Ni F, Jin J, Wu Y, Huang Y, Ye X, Shen X, Ying Y, Chen J, et al. BNC1 deficiency-triggered ferroptosis through the NF2-YAP pathway induces primary ovarian insufficiency. Nat Commun. 2022;13(1):5871.
9. Xu Z, Li H, Yu X, Luo J, Zhang Z. Clinical characterization of hemophagocytic lymphohistiocytosis caused by immune checkpoint inhibitors: a review of published cases. Hematology. 2024;29(1): 2340144.
10. Konen JM, Wu H, Gibbons DL. Immune checkpoint blockade resistance in lung cancer: emerging mechanisms and therapeutic opportunities. Trends Pharmacol Sci. 2024;45(6):520–36.
11. Kong X, Zhang J, Chen S, Wang X, Xi Q, Shen H, Zhang R. Immune checkpoint inhibitors: breakthroughs in cancer treatment. Cancer Biol Med. 2024;21(6):451–72.
12. Emens LA, Romero PJ, Anderson AC, Bruno TC, Capitini CM, Collyar D, Gulley JL, Hwu P, Posey AD Jr, Silk AW, et al. Challenges and opportunities in cancer immunotherapy: a Society for Immunotherapy of Cancer (SITC) strategic vision. J Immunother Cancer. 2024;12(6):e009063.
13. Yin N, Li X, Zhang X, Xue S, Cao Y, Niedermann G, Lu Y, Xue J. Development of pharmacological immunoregulatory anti-cancer therapeutics: current mechanistic studies and clinical opportunities. Signal Transduct Target Ther. 2024;9(1):126.
14. Gao H, Gao L, Wang W. Advances in the cellular immunological pathogenesis and related treatment of primary ovarian insufficiency. Am J Reprod Immunol. 2022;88(5): e13622.
15. Hu F, Zhou X, Jiang Y, Huang X, Sheng S, Li D. Effect of myrcene on Th17/Treg balance and endocrine function in autoimmune premature ovarian insufficiency mice through the MAPK signaling pathway. Protein Pept Lett. 2022;29(11):954–61.
16. Dai F, Liu H, He J, Wu J, Yuan C, Wang R, Yuan M, Yang D, Deng Z, Wang L, et al. Model construction and drug therapy of primary ovarian insufficiency by ultrasound-guided injection. Stem Cell Res Ther. 2024;15(1):49.
17. Zhang S, Yahaya BH, Pan Y, Liu Y, Lin J. Menstrual blood-derived endometrial stem cell, a unique and promising alternative in the stem cell-based therapy for chemotherapy-induced premature ovarian insufficiency. Stem Cell Res Ther. 2023;14(1):327.
18. Ling L, Feng X, Wei T, Wang Y, Wang Y, Wang Z, Tang D, Luo Y, Xiong Z. Human amnion-derived mesenchymal stem cell (hAD-MSC) transplantation improves ovarian function in rats with premature ovarian insufficiency (POI) at least partly through a paracrine mechanism. Stem Cell Res Ther. 2019;10(1):46.
19. Kim HK, Kim TJ. Current status and future prospects of stem cell therapy for infertile patients with premature ovarian insufficiency. Biomolecules. 2024;14(2):242.
20. Day JR, David A, Barbosa MGM, Brunette MA, Cascalho M, Shikanov A. Encapsulation of ovarian allograft precludes immune rejection and promotes restoration of endocrine function in immune-competent ovariectomized mice. Sci Rep. 2019;9(1):16614.
21. Zhang S, Zhu D, Li Z, Huang K, Hu S, Lutz H, Xie M, Mei X, Li J, Neal-Perry G, et al. A stem cell-derived ovarian regenerative patch restores ovarian function and rescues fertility in rats with primary ovarian insufficiency. Theranostics. 2021;11(18):8894–908.
22. Wang G, Li J, Bojmar L, Chen H, Li Z, Tobias GC, Hu M, Homan EA, Lucotti S, Zhao F, et al. Tumour extracellular vesicles and particles induce liver metabolic dysfunction. Nature. 2023;618(7964):374–82.
23. Zhou G, Gu Y, Zhou F, Zhang H, Zhang M, Zhang G, Wu L, Hua K, Ding J. Adipocytes-derived extracellular vesicle-miR-26b promotes apoptosis of cumulus cells and induces polycystic ovary syndrome. Front Endocrinol (Lausanne). 2021;12: 789939.
24. Dai W, Xu B, Ding L, Zhang Z, Yang H, He T, Liu L, Pei X, Fu X. Human umbilical cord mesenchymal stem cells alleviate chemotherapy-induced premature ovarian insufficiency mouse model by suppressing ferritinophagy-mediated ferroptosis in granulosa cells. Free Radic Biol Med. 2024;220:1–14.
25. Liu S, Wang Y, Yang H, Tan J, Zhang J, Zi D. Pyrroloquinoline quinone promotes human mesenchymal stem cell-derived mitochondria to improve premature ovarian insufficiency in mice through the SIRT1/ATM/p53 pathway. Stem Cell Res Ther. 2024;15(1):97.
26. Sadeghi S, Mosaffa N, Huang B, Ramezani Tehrani F. Protective role of stem cells in POI: current status and mechanism of action, a review article. Heliyon. 2024;10(1): e23271.
27. Dinh B, Hoeksema MA, Spann NJ, Rendler J, Cobo I, Glass CK, Yeang C. Isolation and Cryopreservation of Highly Viable Human Peripheral Blood Mononuclear Cells From Whole Blood: A Guide for Beginners. J Vis Exp. 2024;(212).
28. Liu D, Tu X, Huang C, Yuan Y, Wang Y, Liu X, He W. Adoptive transfers of CD4(+) CD25(+) Tregs partially alleviate mouse premature ovarian insufficiency. Mol Reprod Dev. 2020;87(8):887–98.
29. Ye X, Lin Y, Ying Y, Shen X, Ni F, Wang F, Chen J, Zhao W, Yu X, Zhang D, et al. Human amniotic epithelial stem cells alleviate autoimmune premature ovarian insufficiency in mice by targeting granulosa cells via AKT/ERK pathways. Stem Cell Rev Rep. 2024;20(6):1618–35.
30. Chen H, Song L, Xu X, Han Z, Peng F, Zhang Q, Liu C, Liang X. The effect of icariin on autoimmune premature ovarian insufficiency via modulation of Nrf2/HO-1/Sirt1 pathway in mice. Reprod Biol. 2022;22(2): 100638.
31. Grohmann C, Magtoto CM, Walker JR, Chua NK, Gabrielyan A, Hall M, Cobbold SA, Mieruszynski S, Brzozowski M, Simpson DS, Dong H, Dorizzi B, Jacobsen AV, Morrish E, Silke N, Murphy JM, Heath JK, Testa A, Maniaci C, Ciulli A, Lessene G, Silke J, Feltham R. Development of NanoLuc-targeting protein degraders and a universal reporter system to benchmark tag-targeted degradation platforms. Nat Commun. 2022;13(1):2073.
32. Yang Z, Zhang Z, Li L, Jing Z, Ma Y, Lan T, Li Y, Lin Z, Fang W, Zhang J, et al. Bioengineered artificial extracellular vesicles presenting PD-L1 and Gal-9 ameliorate new-onset type 1 diabetes. Diabetes. 2024;73(8):1325–35.
33. Mondal SK, Haas D, Han J, Whiteside TL. Small EV in plasma of triple negative breast cancer patients induce intrinsic apoptosis in activated T cells. Commun Biol. 2023;6(1):815.
34. Zhu Z, Zhang Y, Zhang Y, Zhang H, Liu W, Zhang N, Zhang X, Zhou G, Wu L, Hua K, et al. Exosomes derived from human umbilical cord mesenchymal stem cells accelerate growth of VK2 vaginal epithelial cells through MicroRNAs in vitro. Hum Reprod. 2019;34(2):248–60.
35. Han M, Yang H, Lu X, Li Y, Liu Z, Li F, Shang Z, Wang X, Li X, Li J, et al. Three-dimensional-cultured MSC-derived exosome-hydrogel hybrid microneedle array patch for spinal cord repair. Nano Lett. 2022;22(15):6391–401.
36. Park HS, Chugh RM, Seok J, Cetin E, Mohammed H, Siblini H, Liakath Ali F, Ghasroldasht MM, Alkelani H, Elsharoud A, et al. Comparison of the therapeutic effects between stem cells and exosomes in primary ovarian insufficiency: as promising as cells but different persistency and dosage. Stem Cell Res Ther. 2023;14(1):165.
37. Mi X, Jiao W, Yang Y, Qin Y, Chen ZJ, Zhao S. HGF secreted by mesenchymal stromal cells promotes primordial follicle activation by increasing the activity of the PI3K-AKT signaling pathway. Stem Cell Rev Rep. 2022;18(5):1834–50.
38. Zhou Y, Li Q, You S, Jiang H, Jiang L, He F, Hu L. Efficacy of mesenchymal stem cell-derived extracellular vesicles in the animal model of female reproductive diseases: a meta-analysis. Stem Cell Rev Rep. 2023;19(7):2299–310.
39. Yang Z, Zhang Z, Li L, Jing Z, Ma Y, Lan T, Li Y, Lin Z, Fang W, Zhang J et al: Bioengineered artificial extracellular vesicles presenting PD-L1 and Gal-9 ameliorate new-onset type 1 diabetes. Diabetes. 2024;73(8):1325–1335.
40. Chen C, Sun M, Wang J, Su L, Lin J, Yan X. Active cargo loading into extracellular vesicles: highlights the heterogeneous encapsulation behaviour. J Extracell Vesicles. 2021;10(13): e12163.
41. Wang X, Hu S, Zhu D, Li J, Cheng K, Liu G. Comparison of extruded cell nanovesicles and exosomes in their molecular cargos and regenerative potentials. Nano Res. 2023;16(5):7248–59.
42. Liu C, He D, Li L, Zhang S, Wang L, Fan Z, Wang Y. Extracellular vesicles in pancreatic cancer immune escape: emerging roles and mechanisms. Pharmacol Res. 2022;183: 106364.
43. Wang L, Qi C, Cao H, Zhang Y, Liu X, Qiu L, Wang H, Xu L, Wu Z, Liu J, Wang S, Kong D, Wang Y. Engineered Cytokine-Primed Extracellular Vesicles with High PD-L1 Expression Ameliorate Type 1 Diabetes. Small. 2023;19(38):e2301019.
44. Liu C, Wang Y, Li L, He D, Chi J, Li Q, Wu Y, Zhao Y, Zhang S, Wang L, Fan Z, Liao Y. Engineered extracellular vesicles and their mimetics for cancer immunotherapy. J Control Release. 2022;349:679–698.
45. Fan Y, Pionneau C, Cocozza F, Boëlle PY, Chardonnet S, Charrin S, Théry C, Zimmermann P, Rubinstein E. Differential proteomics argues against a general role for CD9, CD81 or CD63 in the sorting of proteins into extracellular vesicles. J Extracell Vesicles. 2023;12(8):e12352.
46. Fan Y, Pionneau C, Cocozza F, Boëlle PY, Chardonnet S, Charrin S, Théry C, Zimmermann P, Rubinstein E. Differential proteomics argues against a general role for CD9, CD81 or CD63 in the sorting of proteins into extracellular vesicles. J Extracell Vesicles. 2023;12(8): e12352.

47. Corso G, Heusermann W, Trojer D, Görgens A, Steib E, Voshol J, Graff A, Genoud C, Lee Y, Hean J, et al. Systematic characterization of extracellular vesicle sorting domains and quantification at the single molecule - single vesicle level by fluorescence correlation spectroscopy and single particle imaging. J Extracell Vesicles. 2019;8(1):1663043.
48. Silva AM, Lázaro-Ibáñez E, Gunnarsson A, Dhande A, Daaboul G, Peacock B, Osteikoetxea X, Salmond N, Friis KP, Shatnyeva O, et al. Quantification of protein cargo loading into engineered extracellular vesicles at single-vesicle and single-molecule resolution. J Extracell Vesicles. 2021;10(10): e12130.
49. Chen J, Zhang E, Wan Y, Huang T, Wang Y, Jiang H. A quick and innovative pipeline for producing chondrocyte-homing peptide-modified extracellular vesicles by three-dimensional dynamic culture of hADSCs spheroids to modulate the fate of remaining ear chondrocytes in the M1 macrophage-infiltrated microenvironment. J Nanobiotechnol. 2024;22(1):300.
50. Hung ME, Leonard JN. A platform for actively loading cargo RNA to elucidate limiting steps in EV-mediated delivery. J Extracell Vesicles. 2016;5:31027.
51. Daniels RW, Rossano AJ, Macleod GT, Ganetzky B. Expression of multiple transgenes from a single construct using viral 2A peptides in Drosophila. PLoS One. 2014;9(6):e100637.
52. Khosravi GR, Mostafavi S, Bastan S, Ebrahimi N, Gharibvand RS, Eskandari N. Immunologic tumor microenvironment modulators for turning cold tumors hot. Cancer Commun (Lond). 2024;44(5):521–53.
53. Shao C, Yan X, Pang S, Nian D, Ren L, Li H, Sun J. Bifunctional molecular probe targeting tumor PD-L1 enhances anti-tumor efficacy by promoting ferroptosis in lung cancer mouse model. Int Immunopharmacol. 2024;130: 111781.
54. Taghiloo S, Allahmoradi E, Ebadi R, Tehrani M, Hosseini-Khah Z, Janbabaei G, Shekarriz R, Asgarian-Omran H. Upregulation of galectin-9 and PD-L1 immune checkpoints molecules in patients with chronic lymphocytic leukemia. Asian Pac J Cancer Prev. 2017;18(8):2269–74.
55. Lin X, Kang K, Chen P, Zeng Z, Li G, Xiong W, Yi M, Xiang B. Regulatory mechanisms of PD-1/PD-L1 in cancers. Mol Cancer. 2024;23(1):108.
56. Smith BC, Tinkey RA, Brock OD, Mariam A, Habean ML, Dutta R, Williams JL. Astrocyte interferon-gamma signaling dampens inflammation during chronic central nervous system autoimmunity via PD-L1. J Neuroinflammation. 2023;20(1):234.
57. Hou M, Wei Y, Zhao Z, Han W, Zhou R, Zhou Y, Zheng Y, Yin L. Immunoengineered nanodecoys for the multi-target anti-inflammatory treatment of autoimmune diseases. Adv Mater. 2022;34(12): e2108817.
58. Zhang X, Kang Y, Wang J, Yan J, Chen Q, Cheng H, Huang P, Gu Z. Engineered PD-L1-expressing platelets reverse new-onset type 1 diabetes. Adv Mater. 2020;32(26):e1907692.
59. Ma Y, Meng F, Lin Z, Chen Y, Lan T, Yang Z, Diao R, Zhang X, Chen Q, Zhang C, et al. Bioengineering platelets presenting PD-L1, galectin-9 and BTLA to ameliorate type 1 diabetes. Adv Sci (Weinh). 2025;12:e2501139.

Publisher's Note